AGU PUBLICATIONS

JGR

Journal of Geophysical Research: Oceans

RESEARCH ARTICLE

10.1002/2015JC011025

Short wind waves on the ocean: Long-wave and wind-speed dependences

William J. Plant[1]

[1]Applied Physics Laboratory, University of Washington, Seattle, Washington, USA

Key Points:
- Frequency spectra of short waves vary more with long-wave orbital velocity than wavenumber spectra
- Mean-square slopes of ocean waves modeled with long-wave advection agree with Cox and Munk's data
- Mean-square slopes depend on the maximum frequency and wavenumber and on significant wave height

Correspondence to:
W. J. Plant,
plant@apl.washington.edu

Citation:
Plant, W. J. (2015), Short wind waves on the ocean: Long-wave and wind-speed dependences, *J. Geophys. Res. Oceans*, *120*, doi:10.1002/2015JC011025.

Received 3 JUN 2015
Accepted 25 AUG 2015
Accepted article online 27 AUG 2015

Abstract This second paper of our set on short wind waves on the ocean utilizes the wavenumber-frequency spectrum of short wave heights, F(k,f), derived in our previous paper to investigate kinematic effects on the dependence of the frequency spectrum, F(f), and the wavenumber spectrum, F(k), on long-wave height. We show that the model predicts that neither F(f) nor F(k) are exactly power law functions of their independent variables and that F(f) varies with significant wave height much more than F(k) does. After calibrating the model against wave gauges, we also investigate the dependence of mean-square-slopes (mss), mean-square heights (msh) and root-mean-square orbital velocities (rmsv) of short ocean waves on wind speed and maximum frequency or wavenumber. We use data from the wire wave gauges on University of Miami's Air-Sea Interaction Spar (ASIS) buoy for calibration purposes. Frequency spectra from the wave gauges begin to be affected by noise at about 2.5 Hz. Therefore, above 1 Hz, we utilize F(f) from the modeled F(k,f) to extend the frequency dependence up to 180 Hz. We set modeled spectral densities by matching measured spectra at 1 Hz. Using the calibrated F(f,k), we are able to estimate the average value of the total mss, for long and short waves, and its upwind and crosswind components up to 180 Hz for a variety of wind speeds. The average mss values are in good agreement with the measurements of Cox and Munk [1954], although the upwind and crosswind components agree less well.

1. Introduction

In this second paper of our series on short wind waves on the ocean, we utilize the wavenumber-frequency spectrum of short-wave heights, F(k,f), derived in our first paper [*Plant*, 2015] to examine the dependence on significant wave height, Hs, of short-wave-height spectra as functions of wavenumber, k, and frequency f: F(k) and F(f). For brevity, we will refer to these spectra as the wavenumber-frequency spectrum, the wavenumber spectrum, and the frequency spectrum, respectively. We also calibrate our spectra using wire wave gauge measurements to examine the dependence of mean-square slopes, mss, mean-square heights, msh, and root-mean-square velocities, rmsv on wind speed, maximum frequency, and maximum wavenumber.

Measurements of the frequency dependence of F(f) have indicated that it decreases as approximately f^{-4} up to frequencies of about 15–20 Hz [*Toba*, 1973; *Mitsuyasu*, 1977; *Gotwols and Irani*, 1980; *Stolte*, 1984; *Wang and Hwang*, 2004]. Measurements of F(k) have shown that it decreases as approximately k^{-3} [*Lawner and Moore*, 1984; *Banner*, 1990; *Elfouhaily, et al*., 1997; *Plant*, 2002] up to wavenumbers approaching 2000 rad/m.

A variety of techniques have been used to measure the mean-square slopes of ocean waves. By far the most famous measurements of mss were made by *Cox and Munk* [1954] using photographs of sun glitter off the ocean surface. These measurements are the gold standard of mss measurements having held a premier position in air-sea interaction studies for over 60 years. Other measurements of the mss have been made using the observed roll off of microwave backscattering cross sections at low incidence angles [*Jackson et al*., 1992; *Walsh et al*., 1998, *Vandemark et al*., 2004]. The minimum wavelength of waves included in radar-produced mss values depends on the microwave frequency, decreasing as this frequency increases. Lasers and wave gauge arrays on buoys and wave followers have also been used to measure mss values on the ocean. Generally, these studies have yielded either overall average values of the mss at various wind speeds or the values in restricted ranges of wave numbers [*Wang and Hwang*, 2004; *Hwang*, 2005].

Measurements of mean-square heights (msh) and velocities (msv) of short-waves on the ocean are much less common than those of mean-square slopes because of the large effect of dominant waves on these

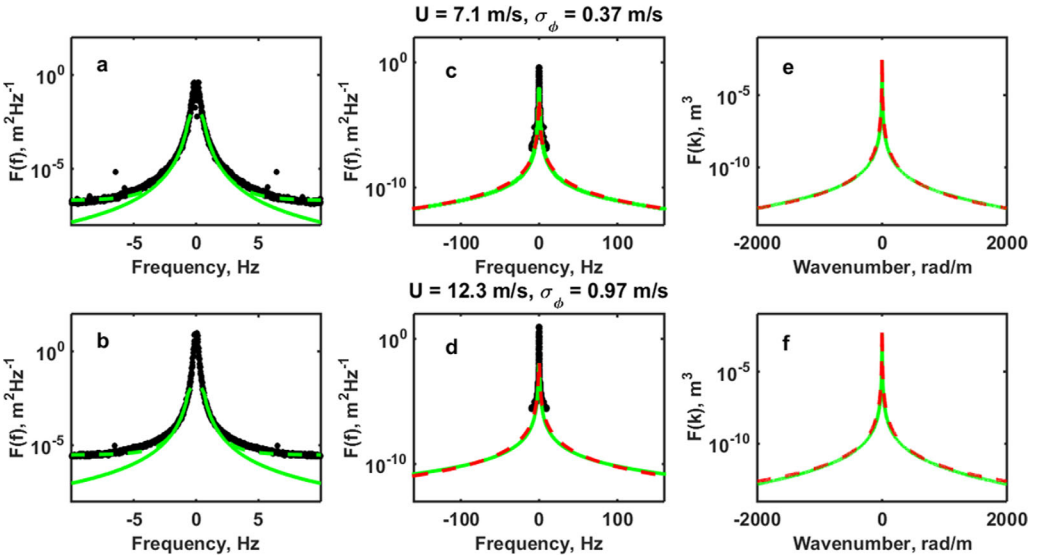

Figure 1. (a-d) Frequency spectra, F(f), and (e, f) wavenumber spectra, F(k), measured and modeled. Black = measured frequency spectra, solid green = calibrated, modeled (a-d) F(f) or (e, f) F(k), (a, b) dashed green = calibrated, modeled F(f) + noise, (a) noise = 1.8×10^{-7} m^2/Hz, (b) noise = 2.9×10^{-6} m^2/Hz, (c) Dashed red = 4×10^{-5} $f^{-3.3}$ m^2/Hz, (d) Dashed red = 6×10^{-4} $f^{-3.5}$ m^2/Hz, (e) Dashed red = 0.008 $k^{-3.25}$ m^3, (f) Dashed red = 0.02 $k^{-3.3}$ m^3. U is wind speed and σ_φ is the standard deviation of long-wave orbital velocities determined by low-pass filtering.

values. Measurements of mean-square height are generally somewhat limited by sampling rates and sensitivities of sensors, although these may not be too serious due to the rapid decrease of wave-height spectra with frequency. Mean-square velocities are of interest for interpreting the width of Doppler spectra in microwave backscatter from the ocean and have generally been deduced from such measurements [*Plant et al.*, 1994]. These Doppler bandwidths determine the azimuthal resolution of synthetic aperture radars (SAR) that view the ocean and, therefore, the shortest azimuthally traveling surface ocean wave that SAR can observe.

Here we show that both F(f) and F(k) as well as all three of the mean-square quantities can be determined from the output of a single wire capacitance wave gauge mounted on a spar buoy, assuming that a unimodal sea with a very narrow angular spread at the dominant wave exists and that the angular dependence of the short waves is known. We use measurements from the wave gauges on University of Miami's Air-Sea Interaction Spar (ASIS) buoy to calibrate our modeled F(f) thereby determining both F(f) and F(k) up to very high frequencies and wavenumbers. We investigate the dependence of F(f) and F(k) on Hs at a constant wind speed using the uncalibrated model. We use the wind-speed-dependent, calibrated F(f) and F(k) to investigate the behavior of mean-square-slopes (mss) of all waves on the surface, and mean-square heights (msh) and root-mean-square velocities (rmsv) of short ocean waves as a function of wind speed. Frequency spectra from the wave gauges begin to be affected by noise at about 2.5 Hz. Therefore, we match measured and modeled spectra at 1 Hz, utilizing measured spectra below 1 Hz and modeled F(f) above 1 Hz to extend the frequency dependence up to 180 Hz. This allows us to vary the maximum frequency and wavenumber to which the mean-square values are computed to observe the effect of this maximum frequency and wavenumber on the mean-square values

2. Measurements

Data were supplied to us by Will Drennan of the Rosenstiel School of Marine and Atmospheric Sciences (RSMAS) at the University of Miami. These data came from a four-wire array of capacitance gauges mounted on the Air-Sea Interaction Spar (ASIS) buoy developed by the University of Miami and the Woods Hole Oceanographic Institution [*Graber et al.*, 2000]. The data were collected by RSMAS during the Deep Ocean Gas Exchange Experiment in the Atlantic Ocean in 2007. The gauges were sampled at a 20 Hz rate and wind speeds ranged from approximately 3.5–15 m/s. The wave gauges were arranged in a square array 20 cm on a side. The data had been corrected for buoy motion before we received them. While in principal our results could have been obtained from a single wave gauge, we averaged spectra from the four gauges together to improve the statistical accuracy.

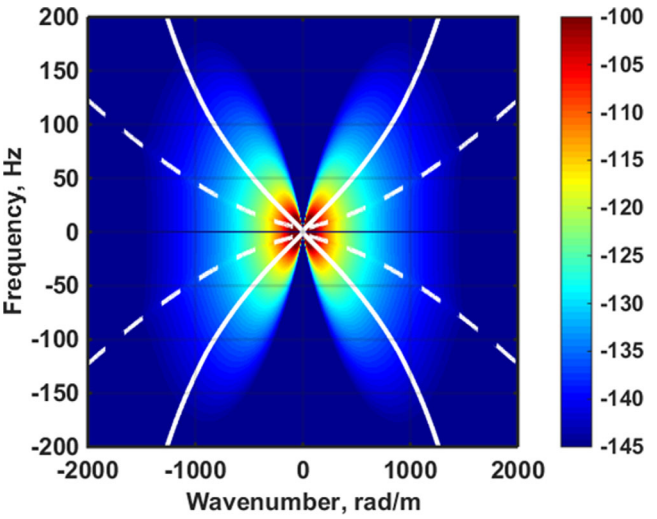

Figure 2. The wavenumber-frequency spectrum derived by *Plant* [2015] shown on a dB scale, 10 $\log_{10}$ (F(k,f)), relative to 1 m^3Hz^{-1}. Dashed white lines are the standard dispersion relation, $f=\frac{1}{2\pi}\sqrt{gk+Tk^3}$. Solid white lines show the spectral mean wavenumber, $k_m(f)$ (see text for definition).

Our data analysis consisted of determining spectra from each of the gauges by Fourier transforming the surface displacement measurements. We then removed any remaining buoy artifacts by setting fft values below 0.075 Hz to 10^{-20}. Figures 1a and 1b show the resulting frequency spectra at two different wind speeds in black. Green curves in Figure 1 are derived from the modeled F(k,f) by integrating over f or k (see Section 3). Spectral densities of the modeled F(f) shown in Figures 1a–1d were set to match the average of measured values between 1 and 1.1 Hz. The level of F(k) was then set by matching $\int F(f)\,df$ and $\int F(k)\,dk$. Red dashed lines are simply power-law fits to the green ones.

3. Modeled Spectra

Plant [2015] derived a form for the short-wave wave-height spectrum, F(**k**,f). There and in this paper, short waves are defined as being those with f >= 0.4 Hz corresponding to k >= 0.64 rad/m. The derived form for F(**k**,f) was

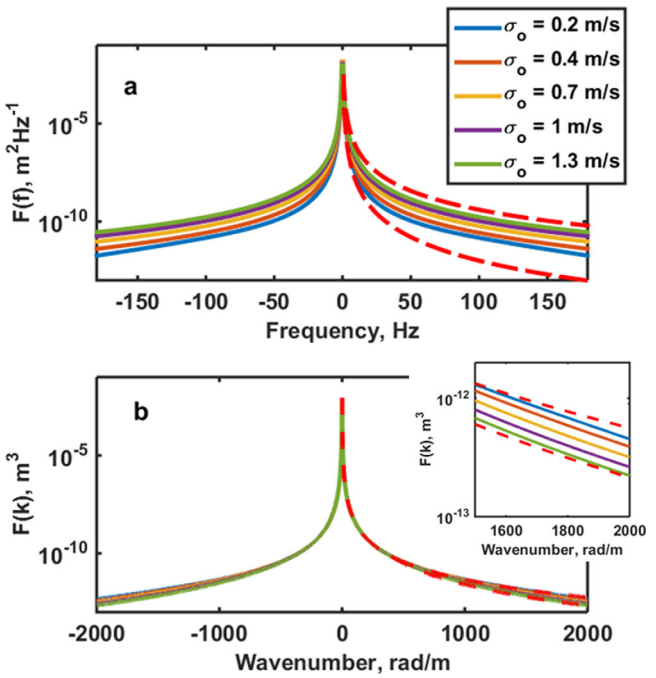

Figure 3. Effect of long-wave orbital velocities on modeled F(f) and F(k). (a) F(f) for various standard deviations of long-wave orbital velocities, $\sigma_{\varphi=0}$. Dashed red lines indicate (top) $f^{-3.4}$ and (bottom) $f^{-4.3}$. (b) F(k) for the same standard deviations. Dashed red lines indicate (top) $k^{-3.25}$ and (bottom) $k^{-3.3}$. The insert is an expansion of the lower right corner. The model was run for a 10.5 m/s wind speed.

$$F(\mathbf{k},f)=\left\{\frac{1.38\times10^{-4}\ W\ P(U_\varphi)}{k^4}\right\}\cos^8(\varphi/2) \quad (1)$$

where W is wind speed, φ is wave angle with respect to the wind, and

$$P(U_\varphi)=\frac{\exp\left\{\frac{-U_\varphi^2}{2\sigma_\varphi^2}\right\}}{\sigma_\varphi\sqrt{2\pi}} \quad (2)$$

where $U_\varphi=U_I\cos\varphi$, U_I is long-wave orbital velocity in the wind direction, $\sigma_\varphi=\sigma_{\varphi=0}\cos\varphi$, and $\sigma_{\varphi=0}$ is the standard deviation of U_I. Values for $\sigma_{\varphi=0}$ may be obtained directly from wave gauge measurements as illustrated by *Plant* [2015] so σ_φ is a function of φ. However, we want to vary U_I so that U_φ satisfies the equation for the wave frequency in the presence of a current, equation (18) of *Plant* [2015]. This equation may be written

$$U_\varphi=\frac{2\pi(f-f_o)}{k}$$

where f_o is the short wave dispersion relation in the absence of currents. For

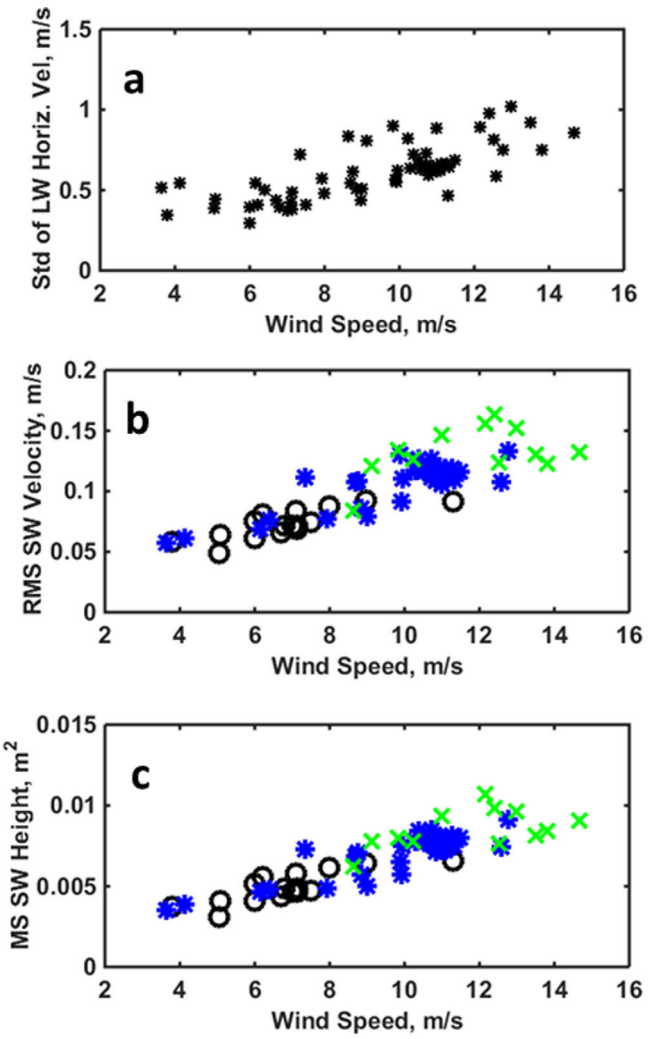

Figure 4. (a) Standard deviation of long-wave orbital velocity, $\sigma_{\varphi=0}$ versus wind speed. (b) Root-mean-squared short wave velocity. c) Mean-square short-wave height versus wind speed. In Figures 4b and 4c, black circles are for $\sigma_{\varphi=0} < 0.5$ m/s, blue asterisks are for 0.5 m/s $\leq \sigma_{\varphi=0} < 0.75$ m/s, and green x's are for 0.75 m/s $\leq \sigma_{\varphi=0}$.

a given f and k, this equation uniquely determines U_φ. Since f_o is not a function of φ, U_φ is also not a function of φ.

Equation (1) assumes a wind sea with a unimodal spectrum with no angular spread at the peak. The wind-speed dependence of $F(\mathbf{k}, f)$ is not necessarily exact and, in fact, requires that the constant carry dimensions of seconds. It would probably be better to replace W by W/f_p, where f_p is the spectral peak frequency. However, this is based only on dimensional analysis so the spectral density obtained from equation (1) cannot be considered to be exact. Therefore in this paper, $F(\mathbf{k}, f)$ was calibrated against wave gauge measurements as described above when investigating wind speed dependences. Figure 2 shows the butterfly shape of F(k,f), the integral of $kF(\mathbf{k}, f)$ over azimuth angle, at a wind speed of 10 m/s. Dashed white lines in this figure are the standard dispersion relation while the solid white lines are spectral mean wavenumbers, which are more relevant for short waves and will be explained below.

Integration of this F(k,f) over k yields F(f), shown as the green curves in Figures 1a–1d while integration over f yields F(k), shown as the green curves in Figures 1e and 1f. Both spectra increase with wind speed as required by the measured spectra. The fitted red dashed curves indicate that the frequency spectra also change their frequency dependence for various long-wave conditions while the wavenumber spectra seem to be less affected.

This behavior is shown for a wider range of long-wave orbital velocities in Figure 3, which shows uncalibrated, modeled F(f) and F(k) for various values of $\sigma_{\varphi=0}$. Figure 3a shows modeled F(f) for various long-wave conditions. The spectra begin to be affected at very low frequencies, approximately 10 Hz. Although they are clearly not power-law forms, they are approximately bounded by $f^{-4.3}$ in low long-wave conditions and $f^{-3.4}$ in high ones. On the other hand, F(k), shown in Figure 3b, goes as approximately k^{-3} all the way out to 400 rad/m then drops a bit faster for high $\sigma_{\varphi=0}$ values. We emphasize that Figure 3 says nothing about the wind speed dependence of F(f) and F(k).

4. Calculation of Azimuthally Averaged Mean-Square Slopes, Heights, and Velocities

Given $F(\mathbf{k}, f)$ we may multiply by k and integrate over φ to get F(k,f), from which azimuthally averaged mean-square values of various quantities associated with short waves may be calculated. Mean-square slopes are given by,

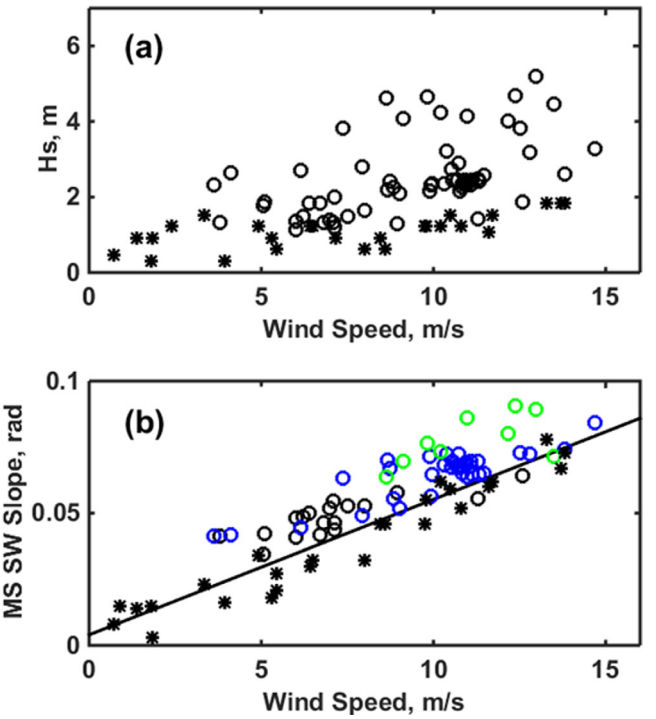

Figure 5. (a) Significant wave heights during our data collection period (o) and when Cox and Munk collected their data (*). (b) Comparison of our azimuthally averaged mean-square slope values with those of Cox and Munk. The solid black line is Cox and Munk's regression fit to their data, shown as black asterisks. The present data are shown as follows: Black open circles are for Hs<2 m, blue open circles are for 2 m <= Hs < 4 m, green open circles are for Hs>= 4 m.

$$\mathrm{mss} = \int k^2 F(k,f)\,dk\,df \tag{3}$$

which we may rewrite as follows,

$$\mathrm{mss} = \int k_m(f)^2\ F(f)\,df \tag{4}$$

where $k_m(f)$ is the spectral mean wavenumber

$$k_m(f)^2 = \frac{\int k^2 F(k,f)\,dk}{F(f)} \tag{5}$$

and,

$$F(f) = \int F(k,f)\,dk. \tag{6}$$

Mean-square heights are simply given by,

$$\mathrm{msh} = \int F(f)\,df. \tag{7}$$

The mean-square short-wave vertical velocity is

$$\left| \frac{\overline{\partial \eta_i(t)}}{\partial t} \right|^2 = 4\pi^2 \int f^2\ F(k,f)\,dk\,df. \tag{8}$$

In deep water, this vertical velocity is equal to and 90° out of phase with the horizontal velocity. Therefore the total mean-square short-wave velocity is,

$$\mathrm{msv} = 8\pi^2 \int f^2\ F(f)\,df. \tag{9}$$

In evaluating these integrals for the entire range of short waves, we let k go from 0.6 to 2000 rad/m and f go from 0.4 to 180 Hz. Expressions for these same quantities for the long waves were given in *Plant* [2015]. They are the same as above except that k_m is replaced by $k_o = (2\pi f)^2/g$ from the long-wave dispersion relation and the integrals go from 0 to 0.4 Hz. For the mss, the value including the long waves is of interest so we add long and short wave mss. For heights and velocities, however, the values of msh and rmsv over all wavenumbers are dominated by the very low wavenumbers, which are highly variable, so we include only the short waves in msh and rmsv.

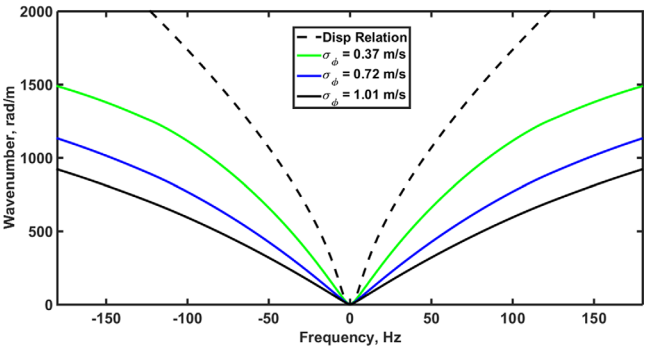

Figure 6. Various wavenumbers versus frequency. Dashed line - Wavenumber from the dispersion relation, k_o. Solid lines—spectral mean wavenumbers, k_m, for various standard deviations of long-wave orbital velocity, $\sigma_{\varphi=0}$. Green: $\sigma_{\varphi=0}$=0.38 m/s. Blue: $\sigma_{\varphi=0}$=0.72 m/s. Black: $\sigma_{\varphi=0}$=1.02 m/s.

Using the frequency spectra calibrated with the wave-gauge data, we may now calculate the wind-speed dependence of these various mean-square quantities. Note that this calibration is irrelevant in computing k_m from equation (5) as long as F(k,f) and F(f) are calibrated in the same manner. Therefore we may use uncalibrated, modeled

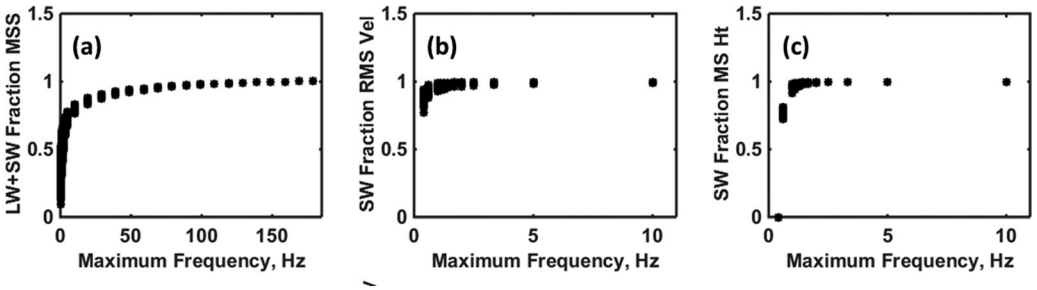

Figure 7. Dependence of (a) mss, (b) rmsv, and (c) msh normalized by their maximum values on the integration limit of frequency.

values of these spectra to compute k_m so k_m does not rely on wave-gauge data. Figure 4 shows the wind speed dependence of msh and rmsv, along with that of $\sigma_{\varphi=0}$. Each point in the three plots corresponds to a different data set. Clearly msh and rmsv increase approximately linearly with wind speed and show little dependence on $\sigma_{\varphi=0}$.

Figure 5 compares our mss values with the data of *Cox and Munk* [1954]. The significant wave heights shown in Figure 5a reached much higher values when the data used here were collected than when Cox and Munk collected their data. The figure shows that our azimuthally averaged mss values agree quite well with those of Cox and Munk when Hs is below 2 m, as was the case when the data of Cox and Munk were collected. As Hs increases, the mss values we calculate also increase, although modestly.

Figure 6 shows why the dependence of mss on Hs is so modest. The figure shows k_o from the dispersion relation as dashed lines and the spectral mean wavenumber k_m from calculations using the short-wave spectrum, F(k,f), as solid lines. Clearly, if k_o, rather than k_m, had been used in equation (4) to calculate mss, the values would have been much too high. Furthermore, Figure 6 shows that at a given frequency, $k_m(f)$ is smaller for larger $\sigma_{\varphi=0}$ values. However, Figure 3a shows that the level of F(f) increases with increasing $\sigma_{\varphi=0}$. These two effects nearly offset each other, causing mss to depend only modestly on Hs. Recall that the long-wave part of the mss is very small.

The spectral mean wavenumbers, k_m, shown in Figure 6 were calculated by integrating up to a wavenumber of 2000 rad/m. This maximum wavenumber is chosen based on a variety of data which show that F(k) begins to fall much more rapidly than k^{-3} just below this wavenumber [*Jähne and Riemer*, 1990; M. A. Donelan, personal communication, 2015]. It is necessary to set this maximum wavenumber since F(k,f) falls as k^{-3} so that the expression for k_m, equation (5), has a logarithmic singularity at infinity.

We can also investigate the dependence of mss, msh, and msv on the maximum frequency by integrating to values less than 180 Hz while still integrating wavenumber up to 2000 rad/m in mss and msh. The dependence of mss, msh, and rmsv normalized by their maximum values on the maximum frequency to which the integral is limited is shown in Figure 7. This figure includes all the data we investigated,

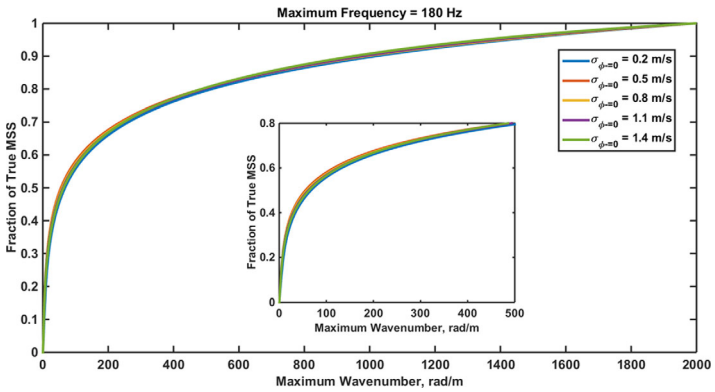

Figure 8. The dependence of the mss normalized by its maximum value on the maximum wavenumber to which equation (3) is integrated following integration over f up to 180 Hz.

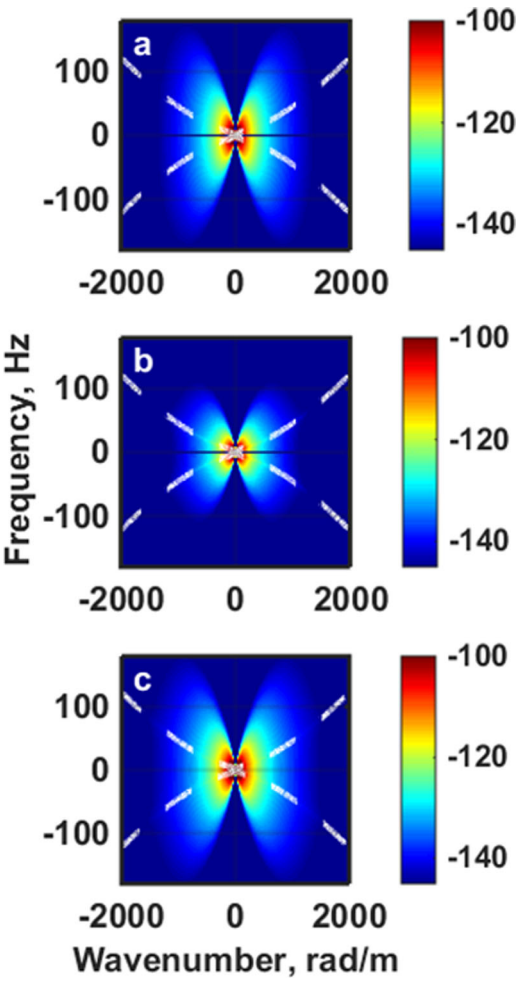

Figure 9. Wavenumber-frequency spectra: (a) Upwind, (b) Crosswind, (c) Total. Dashed curves show the standard dispersion relation. As in Figure 2, the color bars show spectral density on a dB scale relative to 1 m^3Hz^{-1}.

corresponding to all the points in each plot of Figure 4. Note that one must evaluate the mss out to frequencies on the order of 100 Hz before it stops increasing. The values of msh and rmsv, on the other hand, depend mostly on the low frequency part of the short wave spectrum and stop increasing at much lower frequencies. Values of short-wave rms velocities, rmsv, and mean-square heights, msh, are at nearly their maximum values at a maximum frequency of about 2 Hz.

The dependence of mss on the maximum wavenumber to which the integral in equation (3) is evaluated is of special interest. Values of mss can be obtained from near-nadir microwave backscatter measurements but such measurements are only supposed to respond to wavenumbers up to a bit below the microwave number. [*Walsh et al*., 1998; *Jackson et al*., 1992; *Vandemark et al*., 2004]. Therefore, we investigated the behavior of mss when the frequency integral is carried out up to 180 Hz and the maximum wavenumber limit is varied. The results are shown in Figure 7 for several different values of $\sigma_{\varphi=0}$.

Jackson et al. [1992] find that the maximum wavenumber limit for near-nadir radar measurements is 1/3–1/6 times the microwave number. For their Ku-band instrument, this yields a maximum wavenumber to which the radar responds of between about 50 and 100 rad/m. Jackson et al. in their Figure 4b show that the slope of their measured mss wind speed dependence is about 47% of Cox and Munk's. Figure 8 indicates that mss values are 47% of their full value when the wavenumber integral is carried out to about 55–65 rad/m, in good agreement with Jackson's value. However, *Walsh et al*. [1998] have applied similar techniques using a Ka-band radar whose frequency is about 2.6 times that of the radar used by Jackson et al. While the mss versus wind speed shown in *Walsh et al*. [1998, Figure 14], are not linear, they can be approximated by linear fits above about 3 m/s. The average slope of these fits is 46% of Cox and Munk's slope, very similar to those of Jackson et al., as Walsh et al point out. Due to the shorter microwave wavelength, though, the Ka-band radar should measure waves with wavenumbers up to 130–260 rad/m. Again looking at Figure 8, we would expect the Ka-band radar to have measured mss values that were closer to 59–65% of their full values. In fact, *Vandemark et al* [2004] present Ka-band measurements of mss versus wind speed that are 58% of Cox and Munk's values, much closer to what our calculations suggest.

5. Estimation of Upwind and Crosswind Mean-Square Slopes

Our modeling also allows us to calculate the upwind and cross wind mean-square slopes. We have,

$$\mathrm{mss} = \mathrm{mss_u} + \mathrm{mss_c} \tag{10}$$

where the upwind mss is

$$\mathrm{mss}_u = \int k^2 \cos^2\varphi F(\mathbf{k}, f) k\,dk\,df\,d\varphi \equiv \int k^2 F_u(k, f)\,dk\,df \tag{11}$$

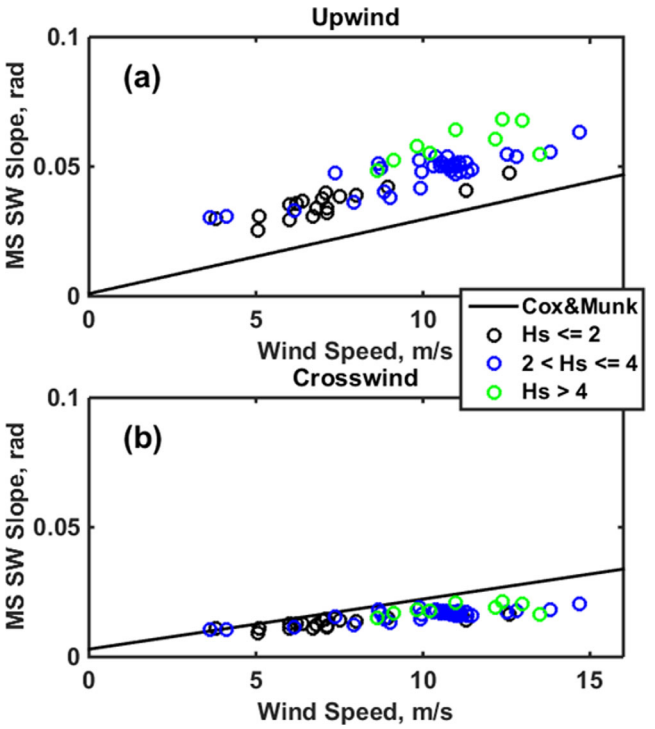

Figure 10. (a) Upwind mean-square slopes from the model compared with Cox and Munk's regression line. (b) Same for crosswind.

and the crosswind value is

$$\mathrm{mss}_c = \int k^2 \sin^2\varphi F(\mathbf{k}, f) k\,dk\,df\,d\varphi = \int k^2 F_c(k, f)\,dk\;df. \tag{12}$$

This immediately allows us to break the spectral mean wavenumber into upwind and crosswind components:

$$k_m(f)^2 = k_{mu}(f)^2 + k_{mc}(f)^2 \tag{13}$$

where

$$k_{mu}(f)^2 = \int k^2 F_u(k, f)\,dk / F(f) \quad \text{and} \quad k_{mc}(f)^2 = \int k^2 F_c(k, f)\,dk / F(f) \tag{14}$$

So

$$\mathrm{mss}_u = \int k_{mu}(f)^2\; F(f)\,df \quad \text{and} \quad \mathrm{mss}_c = \int k_{mc}(f)^2\; F(f)\,df \tag{15}$$

Figure 9 compares $F_c(k, f)$, $F_u(k, f)$, and $F(k, f)$ while Figure 10 compares mss_u and mss_c with Cox and Munk's measurements. Clearly, the values computed here do not agree well with those of Cox and Munk. This may indicate that our assumed short wave angular dependence is incorrect or it could suggest that the long waves are not unidirectional as we have been assuming. Without further information, we pursue this no farther.

6. Conclusion

In this second paper of our series on short waves on the ocean, we have investigated the dependence of the wavenumber spectrum, F(k), the frequency spectrum, F(f), the mean-square slope, mss, the mean-square height, msh, and the root-mean-square velocity, rmsv on wind speed and long-wave orbital velocities. All of these dependent variables refer to azimuthally averaged values and only to the short waves, waves at or above 0.4 Hz in frequency, except for the mss where it was more illuminating to include the longer waves. We also investigated the upwind/crosswind behavior of the mss and found our results to be somewhat different than those of Cox and Munk. We leave to the future the determination whether this indicates a problem in our short wave angular distribution or in our assumption of unidirectionality of long waves.

We found that neither F(f) nor F(k) obeys a strict power-law form over the ranges of frequency and wavenumber that we examined: $0 < f <= 180$ Hz and $0 < k <= 2000$ rad/m. F(f) depends strongly on the orbital velocities of the longer, coexisting waves for all frequencies above about 10 Hz, being higher for higher orbital velocities. F(k), on the other hand, depends much more weakly on long wave orbital velocities, being practically independent of them below 400 rad/m and lower for higher orbital velocities above that wavenumber. This indicates that some care must be taken when discussing the damping of short waves by long [*Gang and Belcher*, 2000]. While we have included no dynamics in our model other than that from the low-frequency data, the kinematic effects discussed here will be present in any measurements and may mask the true dependence of short wave amplitudes on long wave heights.

We found that the mean-square short wave height and the root-mean-square short wave orbital velocity both increase with wind speed approximately linearly and show little dependence on long-wave orbital velocities. We investigated the wind speed dependence of the total mean-squared slope and found it to

agree well with Cox and Munk when the significant wave height, Hs, was about the same as during their measurements. We were able to detect a weak dependence of mss on Hs since our Hs values sometimes exceeded those during Cox and Munk's measurements by a factor of more than two.

Finally, we investigated the dependence of this total mss, as well as msh and rmsv, on the maximum short wave frequency included in integrals. One must integrate mss to much higher frequencies than msh and rmsv in order to get the correct values. We also investigated the dependence of the total mss on the maximum wavenumber included in the integral. We found that our results matched those found in most near-nadir microwave backscatter experiments.

Acknowledgments
The author thanks Will Drennan for supplying the wave gauge. The author is grateful to James Morrison for calling his attention to the problem initially and for finding funding for this work. This research was supported by NASA grant NNX12N01G, ICESat2 Laser Altimetry of the Open Ocean. Data and programs for reproducing the results in this paper are available by contacting the author at plant@apl.washington.edu.

References

Banner, M. L. (1990), Equilibrium spectra of wind waves, *J. Phys. Oceanogr.*, *20*, 966–984.
Cox, C., and W. Munk (1954), Statistics of the sea surface derived from sun glitter, *J. Mar. Res.*, *13*(2), 199–227.
Elfouhaily, T., B. Chapron, K. Katsaros, and D. Vandemark (1997), A unified directional spectrum for long and short wind-driven waves, *J. Geophys. Res.*, *102*, 15,781–15,796.
Gang, C., and S. E. Belcher (2000), Effects of long waves on wind-generated waves, *J. Phys. Oceanogr.*, *30*(9), 2246–2256.
Gotwols, B. L., and G. B. Irani (1980), Optical determination of the phase velocity of short gravity waves, *J. Geophys. Res.*, *85*, 3964–3970.
Graber, H. C., E. A. Terray, M. A. Donelan, W. M. Drennan, J. C. Van Leer, D. B. Peters (2000), ASIS—A new air–sea interaction spar buoy: Design and performance at sea, *J. Atmos. Oceanic Technol.*, *17*, 708–720.
Hwang, P. A. (2005), Wave number spectrum and mean square slope of intermediate-scale ocean surface waves, *J. Geophys. Res.*, *110*, C10029, doi:10.1029/2005JC003002.
Jackson, F. C., W. T. Walton, D. E. Hines, B. A. Walters, and C. Y. Peng (1992), Sea surface mean square slope from Ku-band backscatter data, *J. Geophys. Res.*, *97*, 11,411–11,427.
Jähne, B., and K. S. Riemer (1990), Two-dimensional wave number spectra of small-scale water surface waves, *J. Geophys. Res.*, *95*, 11,531–11,546.
Lawner, R. T., and R. K. Moore (1984), Short gravity and capillary wave spectra from tower-based radar, *IEEE J. Oceanic Eng.*, *9*(5), 317–324.
Mitsuyasu, H. (1977), Measurement of the high-frequency spectrum of ocean surface waves. *J. Phys. Oceanogr.*, *7*, 882–891, doi:10.1175/1520-0485(1977).
Plant, W. J. (2002), A stochastic, multiscale model of microwave backscatter from the ocean, *J. Geophys. Res.*, *107*(C9), 3120, doi:10.1029/2001JC000909.
Plant, W. J. (2015), Short wind waves on the ocean: Wavenumber-frequency spectra, *J. Geophys. Res. Oceans*, *120*, 2147–2158, doi:10.1002/2014JC010586.
Plant, W. J., Keller, W. C., R. A. Petitt, and E. A. Terray (1994), The dependence of microwave backscatter from the sea on illuminated area: Correlation times and lengths, *J. Geophys. Res.*, *99*, 9705–9723.
Stolte, S. (1984), Modulation of short waves by long wind waves and wind, PhD dissertation, 199 pp., Univ. of Hamburg, Hamburg, Germany.
Toba, Y. (1973), Local balance in the air-sea boundary processes. III. On the spectrum of wind waves, *J. Oceanogr. Soc. Jpn.*, *29*, 209–220.
Vandemark, D., B. Chapron. J. Sun, G. H. Crescenti, and H. C. Graber (2004), Ocean wave slope observations using radar backscatter and laser altimeters, *J. Phys. Oceangr.*, *34*, 2825–2845.
Walsh, E. J., D. C. Vandemark, C. A. Friehe, S. P. Burns, D. Khelif, R. N. Swift, and J. F. Scott (1998), Measuring sea surface mean square slope with a 36-GHz scanning radar altimeter, *J. Geophys. Res.*, *103*, 12,587–12,601.
Wang D. W., and P. A. Hwang (2004), The dispersion relation of short wind waves from space–time wave measurements, *J. Atmos. Oceanic Technol.*, *21*, 1936–1945.